Research in Astron. Astrophys. **2011** Vol. **11** No. **1**, 71–90
http://www.raa-journal.org *http://www.iop.org/journals/raa*

Research in Astronomy and Astrophysics

Nonlinear time series analysis of the light curves from the black hole system GRS1915+105

K. P. Harikrishnan[1], Ranjeev Misra[2] and G. Ambika[3]

[1] Department of Physics, The Cochin College, Cochin-682002, India; *kp_hk2002@yahoo.co.in*
[2] Inter University Centre for Astronomy and Astrophysics, Pune-411007, India; *rmisra@iucaa.ernet.in*
[3] Indian Institute of Science Education and Research, Pune-411021, India; *g.ambika@iiserpune.ac.in*

Received 2010 April 14; accepted 2010 July 28

Abstract GRS 1915+105 is a prominent black hole system exhibiting variability over a wide range of time scales and its observed light curves have been classified into 12 temporal states. Here we undertake a complete analysis of these light curves from all the states using various quantifiers from nonlinear time series analysis, such as the correlation dimension (D_2), the correlation entropy (K_2), singular value decomposition (SVD) and the multifractal spectrum ($f(\alpha)$ spectrum). An important aspect of our analysis is that, for estimating these quantifiers, we use algorithmic schemes which we have recently proposed and successfully tested on synthetic as well as practical time series from various fields. Though the schemes are based on the conventional delay embedding technique, they are automated so that the above quantitative measures can be computed using conditions prescribed by the algorithm and without any intermediate subjective analysis. We show that nearly half of the 12 temporal states exhibit deviation from randomness and their complex temporal behavior could be approximated by a few (three or four) coupled ordinary nonlinear differential equations. These results could be important for a better understanding of the processes that generate the light curves and hence for modeling the temporal behavior of such complex systems. To our knowledge, this is the first complete analysis of an astrophysical object (let alone a black hole system) using various techniques from nonlinear dynamics.

Key words: accretion, accretion disks — X-rays: binaries

1 INTRODUCTION

Most of the systems in Nature are described by models which are inherently nonlinear. Since the discovery of *deterministic chaos* a few decades back and the development of various techniques in subsequent years, there remained the exciting prospect of a better understanding of the complex behavior shown by various natural systems in terms of simple nonlinear models. Evidence for low dimensional chaos has been reported - and disputed - not only in physical sciences, but also in many other fields such as physiology, economics and social sciences (Schreiber 1999). Particular attention has been paid to systems producing strange and chaotic attractors, with the word *strange* referring

to metric properties such as fractal dimension and the word *chaotic* representing dynamic properties like exponential divergence of nearby trajectories in phase space. A large number of techniques and measures from nonlinear dynamics and chaos theory are routinely being employed for the analysis of such systems. Excellent text books are now available that give a background knowledge on various methods in nonlinear dynamics (Hilborn 1994; Sprott 2003; Lakshmanan & Rajasekar 2003).

One major difficulty in the analysis of real world systems is that our knowledge regarding the system is usually limited to a single scalar variable recorded as a function of time, called the *time series*. Therefore, a great deal of effort has been devoted to the characterization of underlying attractors reconstructed from time series. The large number of techniques and computational schemes used for this purpose have been discussed in detail by many authors (Kantz & Schreiber 1997; Aberbanel 1996; Hegger et al. 1999).

Among the most important quantifiers used for the analysis of time series data are the correlation dimension (D_2), the correlation entropy (K_2) and the multifractal spectrum. The correlation dimension is often used as a discriminating statistic for hypothesis testing to detect nontrivial structures in the time series. However, when the time series involves colored noise, a better discriminating measure is considered to be K_2 (Kennel & Isabelle 1992). Finally, a complete characterization of the underlying chaotic attractor is done using the generalized dimensions D_q and the $f(\alpha)$ spectrum.

We have recently proposed automated algorithmic schemes (Harikrishnan et al. 2006, 2009a) for the computation of D_2 and K_2 from time series based on the delay embedding technique and applied it successfully to various types of time series data including those from standard chaotic systems, data augmented with white and colored noise and practical time series like EEG and ECG. A generalization of these schemes to compute the multifractal spectrum of a chaotic attractor has also been proposed (Harikrishnan et al. 2010, 2009b). These schemes provide a nonsubjective approach for the characterization of strange attractors inherent in time series.

It should be noted that so far, most of the analysis of the light curves from X-ray binaries and active galactic nuclei (AGNs) have used the conventional techniques such as the power spectrum and distribution. It is widely believed that the light intensity variations are mostly stochastic in nature. For example, it has been shown in the case of the most prominent black hole system, Cygnus X-1, that the observed light curves, at least on certain time scales, are consistent with some static nonlinear transformations of stochastic variations in intensity (Uttley et al. 2005). The authors argue that models based on nonlinear dynamics are not required to explain the data.

However, there is also some analysis based on nonlinearity measures that has been attempted earlier (Voges et al. 1987; Norris & Matilsky 1989; Timmer et al. 2000) on the light curves of some prominent black hole systems, such as Her X-1 and Cygnus X-1. However, these studies have so far not been able to provide conclusive evidence for nontrivial structures in the temporal behavior of such systems. One reason for this has been the limited number of data sets available from such sources with sufficient signal to noise ratio required for such analysis (Norris & Matilsky 1989). The scenario has changed in the last few years as enough data are now available through RXTE observations. Recently, nonlinear time series analysis performed on light intensity data from various astrophysical objects, such as PG 1351+489 (Jevtic et al. 2005), 3C 390–3 (Gliozzi et al. 2005) and 4U 1543–47 (Gliozzi et al. 2010), has provided much more information regarding the system compared to the conventional power spectrum analysis. Attempts have also been made to use the above analysis to differentiate between neutron stars and black holes (Karak et al. 2010) and also between AGNs and black holes (Gliozzi et al. 2010).

Studies on GRS1915+105 have been limited because it became active just over a decade ago. However, the system turns out to be unique among all such sources in that it seems to flip from one state to another continuously with each state having its own temporal variability which is different from the other states. The light curves have been classified into 12 spectroscopic classes based on RXTE observations by Belloni et al. (2000). The nature of the light curves changes completely as the system flips from one state to another. Evidently, pure stochastic processes cannot account for

such qualitative changes in the light curves. Hence, the question naturally arises as to whether some nonlinear deterministic processes are also involved. We do find evidence to support this.

In this paper, we apply the above mentioned automated schemes developed by us to undertake a complete analysis of the X-ray light curves from GRS1915+105. Earlier, a surrogate analysis with D_2 as the discriminating measure has shown that a few of these states manifest the time evolutions analogous to those from low dimensional nonlinear systems with some inherent noise (Misra et al. 2006). This motivates us to undertake an exhaustive numerical analysis of the light curves from the source in all its temporal states using the prominent tools from nonlinear dynamics.

Another motivation for the present investigation has been derived from the fact that the accretion disk in such systems are driven by magneto-hydrodynamic turbulence which is an intrinsically nonlinear process. A model for such a process should be nonlinear and is expected to show qualitative changes in its behavior as a control parameter is varied. For the X-ray radiation from an accretion disk, the rate of mass accretion could possibly be considered as a suitable control parameter. There also exist theoretical models to this effect (Voges et al. 1987; Atmanspacher et al. 1989a) from which it is possible to derive the temporal variability of the X-ray radiation in different regimes of mass accretion rate. Since many of the states of the black hole system under study show nonlinear characters, a complete analysis of the light curves using various nonlinear measures can greatly help in the search for a nonlinear deterministic model to describe the temporal variability of the system.

Our paper is organized as follows: All the quantitative measures used in this paper and the corresponding computational schemes are discussed in detail in the following section. While Sections 2.1 and 2.2 present the computational details for D_2 and K_2, Sections 2.3 and 2.4 focus on SVD and $f(\alpha)$ spectrum respectively. The time series from a standard chaotic system - the Rossler system - is used as an example to illustrate the results in all the cases. The analysis of the X-ray light curves from the black hole system is then undertaken in Section 3 and the conclusions are drawn in Section 4.

2 QUANTITATIVE MEASURES USED FOR THE ANALYSIS

2.1 Correlation Dimension and Surrogate Analysis

Correlation dimension D_2 is often used as a discriminating statistic for hypothesis testing. The conventional method for the calculation of D_2 is the delay embedding method first introduced by Takens (1981), and used effectively by Grassberger & Procaccia (1983), now known as the GP algorithm. More details can be found in Sauer et al. (1991). It creates an embedding space of dimension M with delay vectors constructed by splitting a discretely sampled scalar time series $s(t_i)$ with delay time τ as

$$\boldsymbol{x_i} = [s(t_i), s(t_i + \tau), ..., s(t_i + (M-1)\tau)]\,. \tag{1}$$

The correlation sum is the relative number of points within a distance R from a particular (ith) data point,

$$p_i(R) = \lim_{N_v \to \infty} \frac{1}{N_v} \sum_{j=1, j\neq i}^{N_v} H(R - |\boldsymbol{x_i} - \boldsymbol{x_j}|)\,, \tag{2}$$

where N_v is the total number of reconstructed vectors and H is the Heaviside step function. One then randomly chooses N_c number of centers in the embedded attractor and averages $p_i(R)$ over these randomly selected centers to give the correlation sum

$$C_M(R) = \frac{1}{N_c} \sum_{i}^{N_c} p_i(R)\,. \tag{3}$$

The correlation dimension $D_2(M)$ is then defined to be

$$D_2 \equiv \lim_{R \to 0} d(\log C_M(R))/d(\log(R))\,, \tag{4}$$

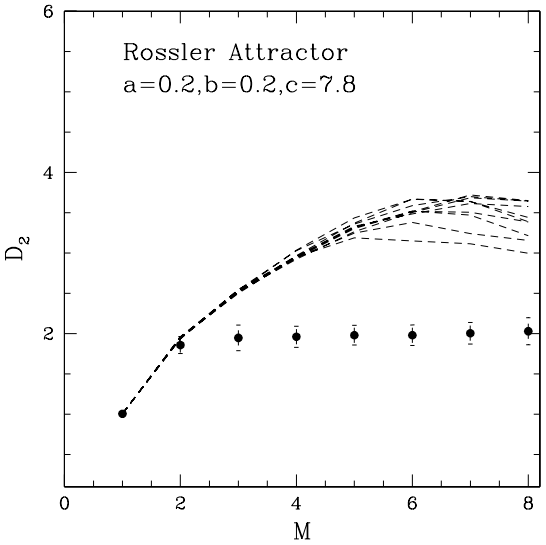

Fig. 1 D_2 values of the Rossler attractor (*with error bars*), as a function of M along with the D_2 values of 20 surrogates (*dashed lines*). All computations are done with 10 000 data points.

which is the scaling index of the variation of $C_M(R)$ with R as $R \to 0$. In practice, a linear part in the $\log C_M(R)$ versus $\log R$ plot is identified subjectively, called the scaling region, and its slope is taken as D_2. However, in our computational scheme, this is done algorithmically, as discussed in detail elsewhere (Harikrishnan et al. 2006), and the scheme computes D_2, with associated error bars, as a function of M. The scheme has also been shown to be suitable for hypothesis testing using surrogate data.

The rationale behind surrogate analysis is to formulate a null hypothesis that the data have been generated by a stationary linear stochastic process, and then attempt to reject it by comparing a suitable measure for the data with appropriate implementations of surrogate data. The method for the generation of surrogate data was originally proposed by Theiler and coworkers (Theiler et al. 1992) with the Amplitude Adjusted Fourier Transform (AAFT) algorithm. However, Schreiber & Schmitz (1996, 2000) have proposed another iterative scheme, known as the IAAFT scheme, which is similar but is reported to be more consistent in representing the null hypothesis (Kugiumtzis 1999) for a wide class of stochastic processes. In this work, we apply this scheme to generate surrogate data sets using the TISEAN package (Hegger et al. 1999).

We first apply the D_2 analysis to different types of data sets, such as standard chaotic time series, pure noise and chaotic data with added noise. The time series from the standard Rossler attractor, with parameter values $a = b = 0.2$ and $c = 7.8$, is used as a reference to test all the computational schemes presented in this work. All computations are done with $10\,000$ data points and 20 surrogates for each data set. In Figure 1, D_2 of the Rossler attractor and surrogates are computed as a function of the embedding dimension M, where as in Figure 2, the same is shown for two pure colored noise data sets with spectral index $s = 1.5$ and 2.0. As expected, the Rossler data show clear deviation from the surrogates while for the latter, the null hypothesis cannot be rejected.

Now the real world data are often contaminated with noise and the question that naturally arises is how much of the noise can suppress the nonlinear component that may be present in the time series. In order to study the effect of noise on D_2 using our scheme, we generate two data sets by

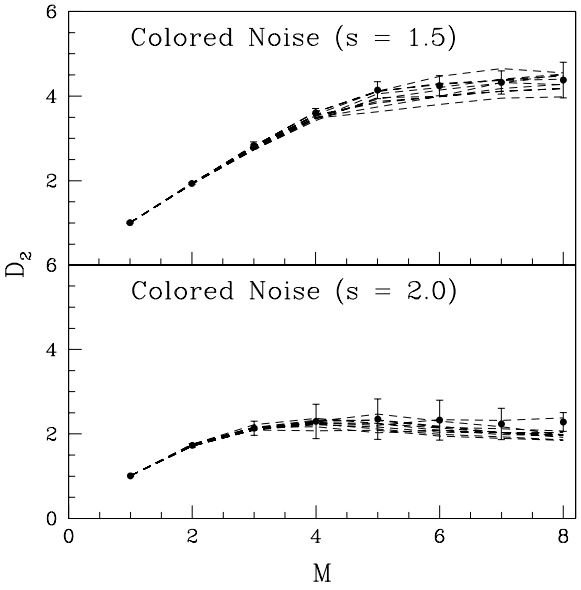

Fig. 2 Upper panel shows the D_2 values of pure colored noise with spectral index $s = 1.5$ as a function of M along with the surrogates. The lower panel shows the same for $s = 2.0$.

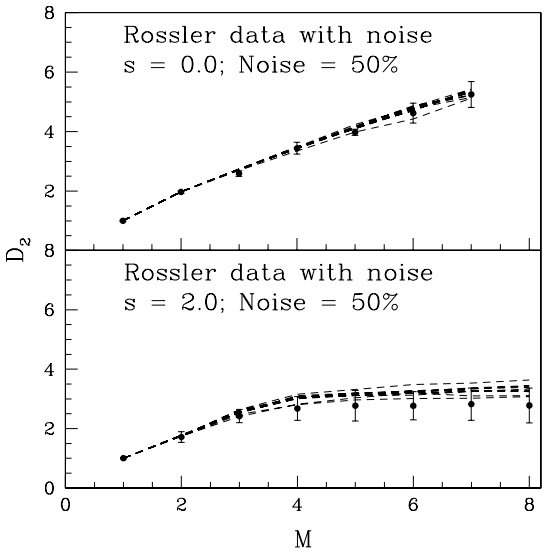

Fig. 3 D_2 values as a function of M for the Rossler attractor data added with 50% white noise ($s = 0.0$) and the same percentage of colored noise ($s = 2.0$) along with their respective surrogates. Note that, in the case of colored noise contamination (*lower panel*), the data values are still below those of the surrogates.

adding 50% white and colored noise (with $s = 2.0$) to the time series from the Rossler attractor. The result of applying our scheme to these data and their surrogates is shown in Figure 3. It is found that when white noise is added to the system, D_2 of the data increases and for a contamination level of $> 20\%$, it is difficult to distinguish between the data and the surrogates. However, for colored noise contamination, the data are distinguishable from the surrogates for an added noise level of up to 50%. Note that 50% noise here means that the noise amplitude is half that of the data. The above results indicate that from a D_2 analysis, it is difficult to distinguish even a moderate amount of noise contamination in chaotic data. A better quantitative measure in such a situation is K_2, to be discussed in the next section.

In order to get a quantification of the differences in the discriminating measure between the data and the surrogates, we use the normalized mean sigma deviation (nmsd), recently proposed by us (Harikrishnan et al. 2006). For D_2, this is computed using the expression

$$\mathrm{nmsd}^2 = \frac{1}{M_{\max} - 1} \sum_{M=2}^{M_{\max}} \Big(\frac{D_2(M) - \langle D_2^{\mathrm{surr}}(M) \rangle}{\sigma_{\mathrm{SD}}^{\mathrm{surr}}(M)} \Big)^2 , \tag{5}$$

where $M_{\max}$ is the maximum embedding dimension for which the analysis is undertaken, $\langle D_2^{\mathrm{surr}}(M) \rangle$ is the average of $D_2^{\mathrm{surr}}(M)$ and $\sigma_{\mathrm{SD}}^{\mathrm{surr}}(M)$ is the standard deviation of $D_2^{\mathrm{surr}}(M)$. We have earlier shown that a value of nmsd < 3.0 implies either white or colored noise domination in the data and the null hypothesis cannot be rejected (see for example Harikrishnan et al. 2006). It is found that for the Rossler attractor data shown in Figure 1, the nmsd = 36.1 and for the two with pure colored noise in Figure 2, the nmsd = 0.68 and 2.0 for s = 1.5 and 2.0 respectively. For data contaminated by noise in Figure 3, the values are 1.8 for white noise and 3.5 for colored noise.

2.2 Correlation Entropy

The use of K_2 has been limited compared to D_2 for the analysis of time series data. However, in cases where time series involve colored noise, K_2 is a more effective discriminating measure compared to D_2 (Redaelli et al. 2002). While D_2 is a geometric measure of the underlying chaotic attractor, K_2 is a dynamic measure representing the rate at which information needs to be created as the chaotic attractor evolves in time (Ott 1993). The standard method for the computation of K_2 is also the delay embedding technique. Since K_2 measures the rate at which the trajectory segments are increased as M increases, it can be related to the correlation sum $C_M(R)$ by the expression

$$C_M(R) \propto e^{-MK_2\Delta t}, \tag{6}$$

where Δt is the time step between successive values in the time series. From above, a formal expression for K_2 can be written as

$$K_2\Delta t = \lim_{R\to 0} \lim_{M\to\infty} \lim_{N\to\infty} (-\log C_M(R)/M) . \tag{7}$$

Alternately, K_2 can also be obtained as

$$K_2\Delta t \equiv \lim_{R\to 0} \lim_{M\to\infty} \lim_{N\to\infty} \log(C_M(R)/C_{M+1}(R)). \tag{8}$$

Our nonsubjective scheme has been extended for the computation of K_2 as well (Harikrishnan et al. 2009a) and we apply that scheme in this work.

Figure 4 shows K_2 for the Rossler attractor as a function of M computed from the time series using our scheme. To show the effect of noise on K_2, we generate four different time series by adding 50% and 100% white as well as colored noise to the Rossler attractor data. The result of applying our scheme to these data sets is shown in Figure 5. It is clear that while the saturated K_2

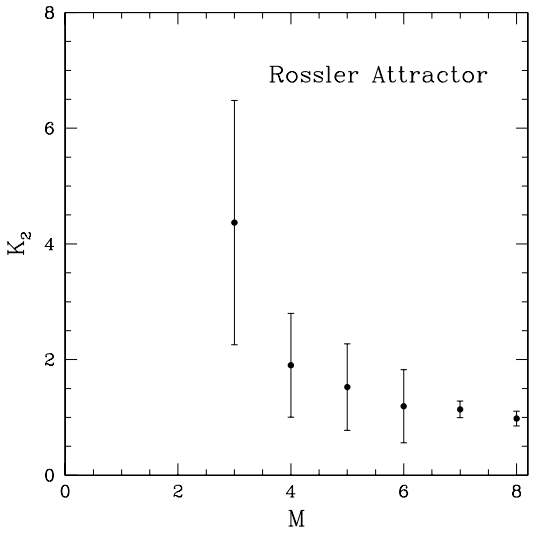

Fig. 4 K_2 values of the Rossler attractor as a function of M computed using our scheme. The values are computed per second and converge very close to the standard value 1.04 ± 0.08.

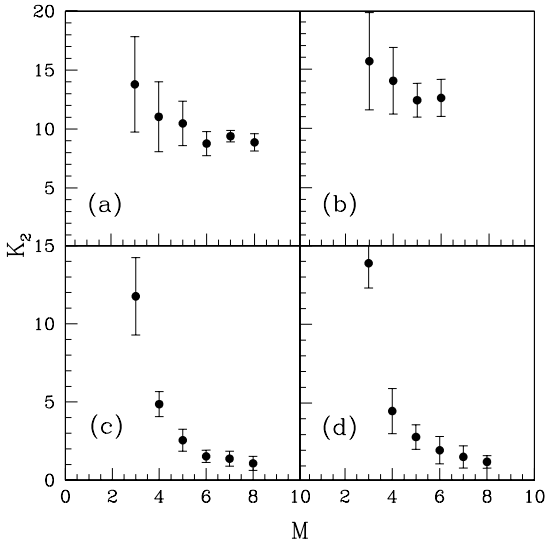

Fig. 5 Variation of K_2 with M for data sets obtained by adding different amounts of white and colored noise to the Rossler attractor data. The upper panel shows the result of addition of (a) 50% and (b) 100% white noise, while the lower panel shows the results with (c) 50% and (d) 100% colored noise with $s = 2.0$. It is clear that while K_2 increases with the addition of white noise, $K_2 \to 0$ as the percentage of colored noise increases.

value increases with the white noise addition, the effect of colored noise is quite the opposite. With the increase in colored noise, the saturated value of $K_2 \rightarrow 0$.

Our scheme can be used for surrogate analysis with K_2 as the discriminating measure as well and nmsd can be computed using a similar expression as Equation (5). We have recently applied this (Harikrishnan et al. 2009a) to the Rossler attractor data with different percentages of white and colored noise added. For 50% white noise contamination, nmsd with K_2 as the discriminating measure is found to be 4.3, while for the same percentage of colored noise, the value is 2.2. Thus, while the white noise contamination can be easily identified through D_2 analysis, the presence of colored noise can be better inferred by computing K_2.

2.3 Singular Value Decomposition

The singular value decomposition (SVD) is another important technique used in nonlinear time series analysis, first proposed by Broomhead & King (1986) and for a recent review, see Athanasiu & Pavlos (2001). The method makes use of a trajectory matrix constructed from the experimental time series with the rows of the matrix constituting the state vectors in the embedding space. It is then diagonalized to find the dominant eigenvalues and eigenvectors which are used to represent the dynamics. The number of dominant eigenvalues determines the minimum number of dimensions required to unfold the complete dynamics and the corresponding eigenvectors give the projections of the reconstructed attractors. With such an SVD projection (also called a BK projection), one can visualize the qualitative nature of the reconstructed attractors. Here we use the standard TISEAN algorithm (Hegger et al. 1999) for the computation of BK projections.

For example, the SVD projection for the Rossler attractor is shown in Figure 6 (upper panel). To show the effect of colored noise on the SVD projection, we also show in Figure 6 (lower panel) the BK projection for the Rossler attractor with 50% added colored noise and a spectral index $s = 2.0$. It is evident that even such a large amount of colored noise does not completely destroy the attractor.

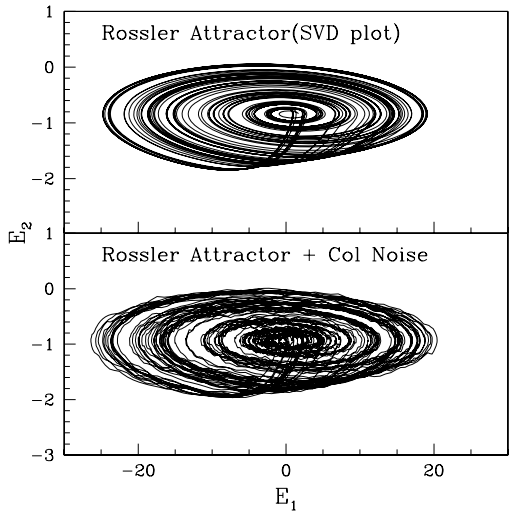

Fig. 6 SVD plot of the pure Rossler attractor (*upper panel*) along with a plot of the attractor obtained by adding 50% colored noise $(s = 2.0)$ to the Rossler attractor time series (*lower panel*).

2.4 Multifractal Spectrum

The interest of the multifractal formalism in connection with dynamical systems rests on the fact that it provides us with a very efficient method to determine the existence of *strange attractors* and allows a statistical description of these sets. A strange or chaotic attractor normally possess a multifractal structure as a result of the stretching and folding of the trajectories in different directions in phase space. Hence they can be characterized by a spectrum of dimensions $D(q)$ (Hentschel & Procaccia 1983), where the index q can vary from $-\infty$ to $+\infty$. The clustered regions of the attractor are characterized by $D(q)$ values with $q > 0$ and rarefied regions by $D(q)$ with $q < 0$, with $D(0)$ giving the simple fractal dimension of the set.

A more convenient method to represent the global scaling properties of the attractor is by a spectrum of singularities characterising the probability measure on the strange attractor. For this, one considers a covering of the attractor with boxes (of edge length ϵ) and assign a probability measure $p_i(\epsilon)$ for the ith box. One can then define a local scaling exponent α_i (called the singularity strength) corresponding to the ith box as

$$\alpha_i = \lim_{\epsilon \to 0} \frac{\log\, p_i(\epsilon)}{\log\, \epsilon}\,. \tag{9}$$

Thus α_i measures how fast the number of points within the ith box decreases as ϵ is reduced. It therefore measures the strength of the singularity as $\epsilon \to 0$.

For a multifractal, α_i can take any value within a range ($\alpha_{\min}$, $\alpha_{\max}$). Suppose we now count the number of boxes N_{α_i} having the same singularity measure α_i, for a given ϵ. Then the variation of $N_{\alpha_i}(\epsilon)$ with ϵ defines the fractal dimension $f(\alpha_i)$ of the set with the same singularity strength α_i. Plotting $f(\alpha_i)$ versus α_i gives the singularity spectrum.

But in practice, one is mainly interested in the range of values of α_i and the smooth profile of the singularity spectrum, by taking α_i as a continuous parameter α, varying smoothly from $\alpha_{\min}$ to $\alpha_{\max}$. If we now count the number of boxes $N_\alpha(\epsilon)$ corresponding to an infinitesimal range of α around α_i within α and $\alpha + d\alpha$, then the variation of $N_\alpha(\epsilon)$ with ϵ can be written as

$$N_\alpha(\epsilon) \propto \epsilon^{-f(\alpha)}\,, \tag{10}$$

where the exponent $f(\alpha)$ represents the fractal dimension of subsets with singularity strength α. The graph of $f(\alpha)$ as a function of α is called the $f(\alpha)$ spectrum which characterizes the global scaling properties of the fractal set as a function of the local scaling exponents α. The transformation from $D(q)$ to $f(\alpha)$ can be shown to be a Legendre transformation; for details, see Halsey et al. (1986) and Atmanspacher et al. (1989b).

To compute the $f(\alpha)$ spectrum from a time series, we first consider the generalized correlation sum given by

$$C_M^q(R) = \Big[\frac{1}{N_c}\sum_i^{N_c}\Big(\frac{1}{N_v}\sum_{j=1, j\neq i}^{N_v} H(R - |\boldsymbol{x_i} - \boldsymbol{x_j}|)\Big)^{q-1}\Big]^{1/(q-1)}\,, \tag{11}$$

where the Heaviside function H counts how many pairs of points at $(\boldsymbol{x_i}, \boldsymbol{x_j})$ are situated within a distance R. The spectrum of dimensions are then determined by the relation

$$D(q) \equiv \lim_{R \to 0} \frac{d\,(\log\, C_M^q(R))}{d\,(\log\, (R))}\,. \tag{12}$$

The average value of D_q with error bar is then calculated from the scaling region by taking different values of R, by extending the numerical procedure discussed above for computing D_2.

In order to determine the $f(\alpha)$ spectrum, we make use of the computational scheme recently proposed by us and applied to several practical time series (Harikrishnan et al. 2009b). The scheme uses an analytical fit for the $f(\alpha)$ function (involving a set of independent parameters) and calculates the corresponding D_q curve using the Legendre transformation equations. This curve is then fitted to the spectrum of D_q values computed from the time series. The best fit curve is found by changing the parameters of the $f(\alpha)$ fit, which is then used to compute the final $f(\alpha)$ spectrum. The algorithmic details of the scheme are presented elsewhere (Harikrishnan et al. 2009b). The multifractal approach has recently been employed in the analysis of several practical time series, an example being the temporal variations of the geomagnetic field (Hongre et al. 1999).

To illustrate our scheme, it is first used to compute the $f(\alpha)$ spectrum of the Rossler attractor. The spectrum of generalized dimensions D_q is computed from the time series taking the embedding dimension $M = 3$. Attempting to compute the $f(\alpha)$ spectrum directly from the D_q values leads to an incomplete $f(\alpha)$ spectrum. This is mainly due to the fact that the errors in the calculation of D_q makes the Legendre transformation numerically impractical because of the reversal of slopes. Hence, our scheme uses a different procedure. The $f(\alpha)$ function is a single valued function defined between the limits of $\alpha_{\min}$ and $\alpha_{\max}$. Since the derivative $f'(\alpha) = df(\alpha)/d\alpha = q$ is also single valued, it follows that $f(\alpha)$ has a single extremum (i.e. a maximum). Moreover, $f(\alpha_{\min}) = f(\alpha_{\max}) = 0$ and $f'(\alpha_{\min})$ and $f'(\alpha_{\max})$ tend to ∞ and $-\infty$ respectively. A simple function which can satisfy all the above necessary conditions is

$$f(\alpha) = A(\alpha - \alpha_{\min})^{\gamma_1}(\alpha_{\max} - \alpha)^{\gamma_2}\,, \tag{13}$$

where A, γ_1, γ_2, $\alpha_{\min}$ and $\alpha_{\max}$ are a set of parameters characterizing a particular $f(\alpha)$ curve. The D_q curve can be computed from this $f(\alpha)$ fit using the inverse Legendre transformation equations for a given set of parameters. It is then fitted to the D_q spectrum computed from the time series. The statistically best D_q fit curve is found by adjusting the parameters of the $f(\alpha)$ function, which is then used to compute the final $f(\alpha)$ spectrum. The D_q spectrum and its best fit curve for the Rossler attractor are shown in Figure 7 and the $f(\alpha)$ spectrum computed from the best fit curve is shown in Figure 8. Having discussed the various measures and schemes for computing them, we now turn to the analysis of the black hole system GRS1915+105.

3 ANALYSIS OF THE BLACK HOLE SYSTEM GRS1915+105

In this section, we apply all the techniques discussed above to analyze the X-ray light curves from the black hole binary GRS1915+105. The temporal properties of the system have been classified into 12 different spectroscopic classes by Belloni et al. (2000) based on the RXTE data. Here we have chosen representative data sets for each class. The light-curve for an observation was obtained from the standard products[1], which provide a 0.125 s time resolution summed over all energy channels. Standard product light curves have been generated using a pipeline which considers standard filtering criteria and use reliable data from the instruments. While standard products may not have an optimal spectral response matrix or a background model, they are more than adequate for light curve analysis, especially for bright sources, like GRS 1915+105, where the background is not important.

The analysis requires continuous data without gaps. For each class, we have extracted two sets of continuous segments for the analysis. The light curves have been generated after rebinning to a time resolution of 0.5 s, resulting in ~ 5200 to 6400 continuous data points for each segment. Light curves with finer time resolutions are more Poisson noise dominated, while larger binning gives less data points. Table 1 gives the observation ID, class, number of data points, etc., of all the light curves used in the analysis. In the last column, we also provide the temporal behavior of the light curve that resulted from our analysis. More details regarding the data, such as average count, expected Poisson noise variation, etc., are given elsewhere (Misra et al. 2004).

[1] *http://heasarc.gsfc.nasa.gov/docs/xte/recipes/stdprod_guide.html*

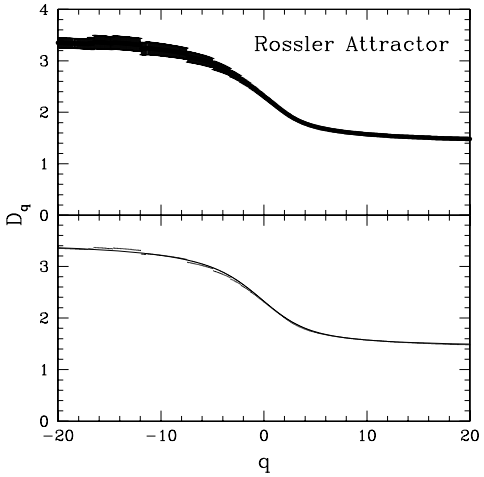

Fig. 7 Upper panel shows the D_q spectrum of the Rossler attractor with error bars, computed from the time series of 10 000 data points. To show the accuracy of the fitting, the D_q values (*points*) are again shown in the lower panel without error bars along with the best fit curve (*continuous line*) computed using our numerical scheme.

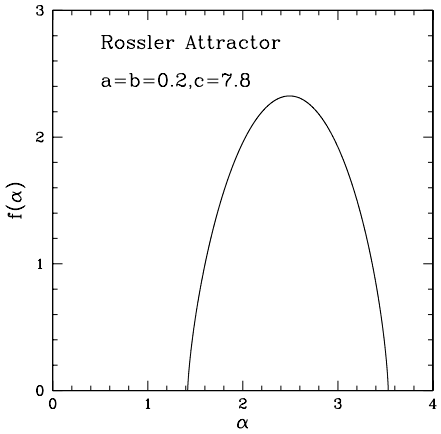

Fig. 8 $f(\alpha)$ spectrum of the Rossler attractor computed from the best fit D_q curve shown in the previous figure.

Figure 9 shows all the 12 light curves used in the analysis, which are labeled by 12 different symbols representing the 12 temporal states of the black hole system. We show only one set of light curves since the second set looks identical for all the states. The system appears to flip from one state to another randomly in time. The classification of Belloni et al. (2000) is based on a detailed analysis of all the light curves from RXTE data using various linear tools. However, it is difficult to differentiate the subtle temporal features between the light curves with the help of the linear tools, such as the power spectrum. For example, in Figure 10, we show the power spectrum for four representative

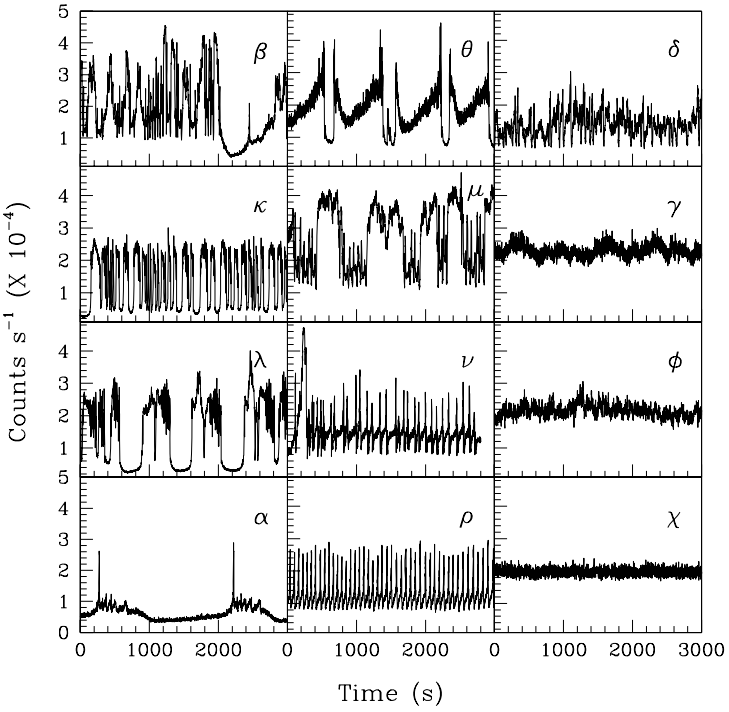

Fig. 9 Light curves from the 12 temporal states of the black hole system GRS1915+105. Only a part of the generated light curve is shown for clarity.

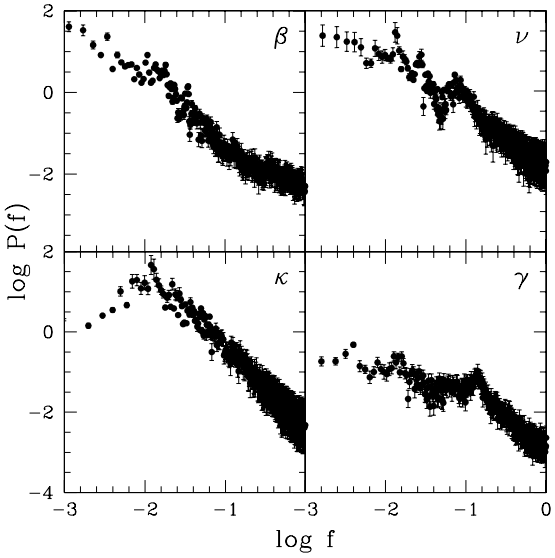

Fig. 10 Power spectrum for the X-ray light curves from GRS 1915+105 in four representative states.

Table 1 Details of the light curves from GRS 1915+105, in all the 12 spectral classes, used for the analysis. For each class, light curves from two Observation IDs have been analyzed, as indicated. The second column gives the number of continuous data points after rebinning. The last column indicates the temporal behavior of the class as obtained from our analysis.

Obs. ID	No. of Data Points	Class	Temporal Behavior
10408–01–10–00	6146		
20402–01–46–00	5504	β	Deterministic Nonlinear
20402–01–45–00	6156		
10408–01–15–00	5764	θ	Deterministic Nonlinear
20402–01–03–00	6244		
20402–01–31–00	5876	ρ	Deterministic Nonlinear
10408–01–40–00	6024		
10408–01–41–00	5312	ν	Deterministic Nonlinear
20187–02–01–00	6010		
20402–01–22–00	5220	α	Deterministic Nonlinear
20402–01–33–00	6240		
20402–01–35–00	6244	κ	Deterministic Nonlinear + Colored Noise
20402–01–37–00	6080		
20402–01–36–00	5648	λ	Deterministic Nonlinear + Colored Noise
10408–01–08–00	5688		
10408–01–34–00	5756	μ	Deterministic Nonlinear + Colored Noise
10408–01–17–00	6010		
20402–01–41–00	5466	δ	White Noise
20402–01–56–00	6324		
20402–01–39–00	6180	γ	White Noise
10408–01–12–00	6286		
10408–01–09–00	5580	ϕ	White Noise
10408–01–22–00	6022		
20402–01–04–00	5382	χ	White Noise

states whose temporal properties are different as compared to our analysis (see Table 1). While β and ν are candidates for deterministic nonlinear behavior, κ is possibly a mixture of nonlinearity and colored noise and γ is purely stochastic. However, these distinctions are barely evident from the power spectral variations, though the γ state appears more like white noise, in agreement with our results. This, once again, emphasizes the importance of methods based on nonlinear time series analysis for a better understanding of the temporal properties of the light curves.

Recently, we applied a surrogate analysis to all these light curves and showed that more than half of these 12 states deviated from purely stochastic behavior (Misra et al. 2006). Here we combine the results of computations of D_2, K_2 and SVD analysis to get a better understanding regarding the nature of these light curves. We have done the surrogate analysis with D_2 and K_2 and the SVD analysis separately for the two sets of light curves. However, here we only show plots from representative light curves from one set since the plots from the second set are similar and the results are qualitatively the same. Figures 11 and 12 show the results of the surrogate analysis, with D_2 as the discriminating measure, on eight different states. Of the states shown in these figures, it is clear that only two states (γ, ϕ) show purely stochastic behavior.

Figure 13 presents the results of the computation of K_2 for six of the above eight states. Since colored noise is also expected in the black hole data, the surrogate analysis has been performed with K_2 as the discriminating measure on all the 12 states. The results are shown in Figure 14 for four of these states. While the behavior of β, θ and γ are consistent with earlier analysis, the behavior of κ suggests that it is contaminated by colored noise.

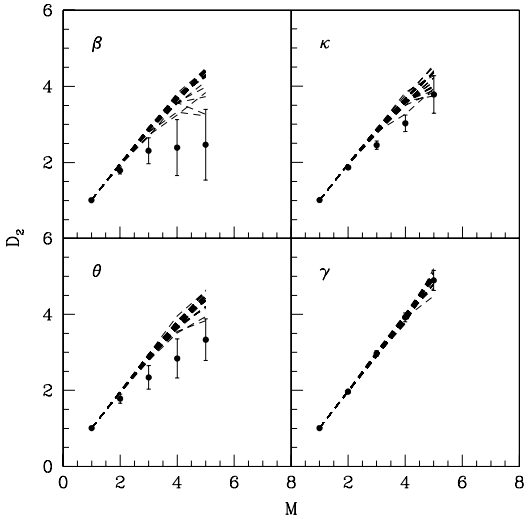

Fig. 11 Surrogate analysis with D_2 as a discriminating measure for the light curves from four states of GRS1915+105. Note that only the γ state is consistent with noise.

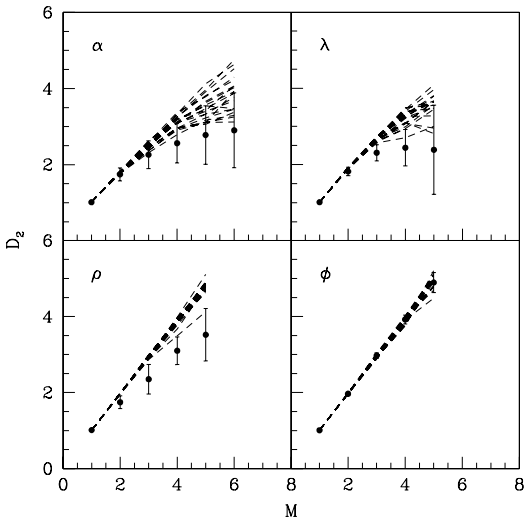

Fig. 12 Same as the previous figure, but with four other states. Again, only one state (ϕ) shows random behavior.

To get a quantitative measure, we now compute nmsd using both D_2 and K_2 as discriminating measures for all the 12 states from the two sets of light curves and the results are shown in Table 2. A careful inspection of the Table reveals the following results. The values of nmsd in the two cases suggest that the temporal properties of the light curves in the two sets are almost identical. Out of the 12 states, four $(\delta, \gamma, \phi, \chi)$ are completely stochastic or white noise. Of the remaining eight states, three (κ, λ, μ) are contaminated by colored noise and the rest ($\beta, \theta, \alpha, \nu$, ρ) show signatures of deterministic nonlinear behavior in their temporal variations. It is generally expected that all the

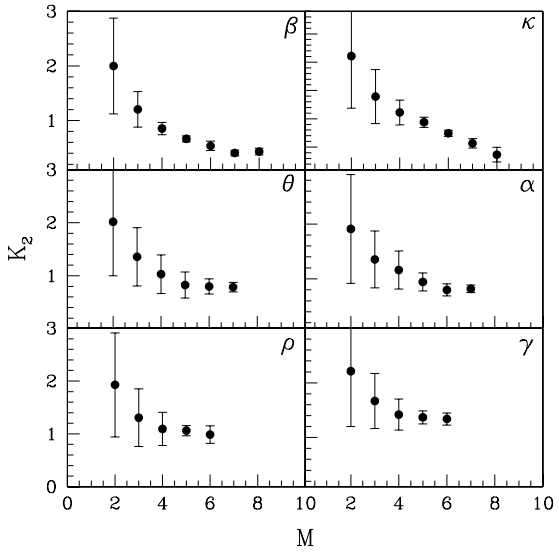

Fig. 13 Variation of K_2 as a function of M for the light curves from six different states of GRS1915+105. While the K_2 values of four states converge much like a low dimensional chaotic system, K_2 for the κ state continues to decrease as M increases, indicating colored noise contamination. Though K_2 for the γ state converges, its value is much higher and closer to that of the white noise.

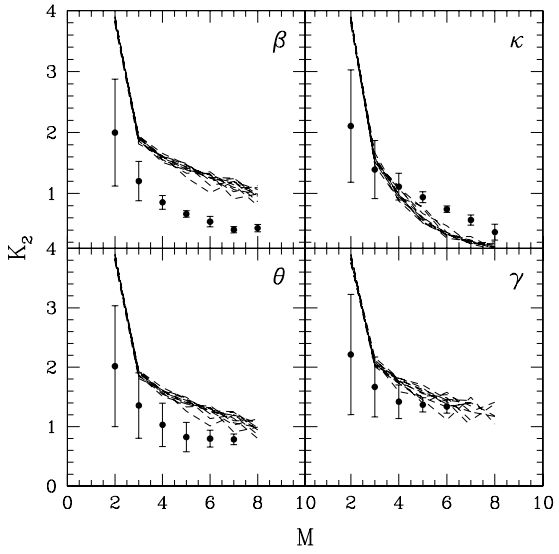

Fig. 14 Surrogate analysis of the light curves from four states of the black hole system with K_2 as the discriminating measure. Note that while data and the surrogates can be distinguished for β and θ, κ and γ behave much like colored noise and white noise respectively.

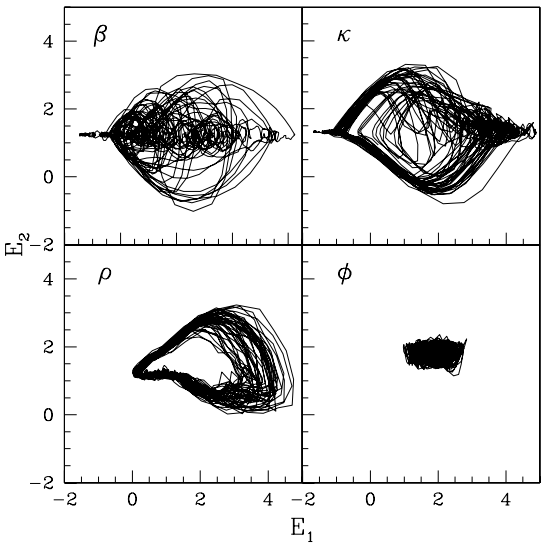

Fig. 15 Plot of the attractors underlying four states of the black hole system reconstructed via SVD analysis. Except for the ϕ state, which behaves similar to white noise, all the others indicate the presence of underlying attractors, with the most interesting being the ρ state.

Table 2 Values of nmsd computed for all the 12 GRS states from the two sets of light curves with D_2 and K_2 as discriminating measures.

GRS state	nmsd (D_2) set 1	nmsd (D_2) set 2	nmsd (K_2) set 1	nmsd (K_2) set 2
β	7.04	9.32	13.74	11.44
θ	10.63	8.59	11.20	10.86
α	8.18	6.71	8.92	6.89
ν	5.94	6.04	6.87	6.35
ρ	11.25	10.83	14.28	12.08
κ	4.64	4.77	3.22	3.54
λ	6.66	6.22	4.57	4.67
μ	4.86	4.90	3.98	3.82
δ	2.32	3.13	1.34	1.68
γ	0.88	1.03	1.83	1.43
ϕ	0.96	0.92	2.12	1.74
χ	0.78	0.73	1.67	1.38

states contain some amount of white noise whose percentage may vary. For example, in the case of the state α, the saturated values of D_2 and K_2 improve significantly as the resolution time is increased from 0.5 s to 1 s. This clearly indicates the presence of Poisson white noise in the data. However, the surrogate analysis with both D_2 and K_2 confirms that the null hypothesis can be rejected for the light curve in the α state.

We next perform an SVD analysis on all the states which clearly show the qualitative nature of the underlying attractors. The plots of attractors for selected states are shown in Figure 15. The most interesting plot is for the ρ state which shows a typical limit cycle type attractor. Also, note that the SVD plot for κ has a nontrivial appearance, even though the surrogate analysis suggested

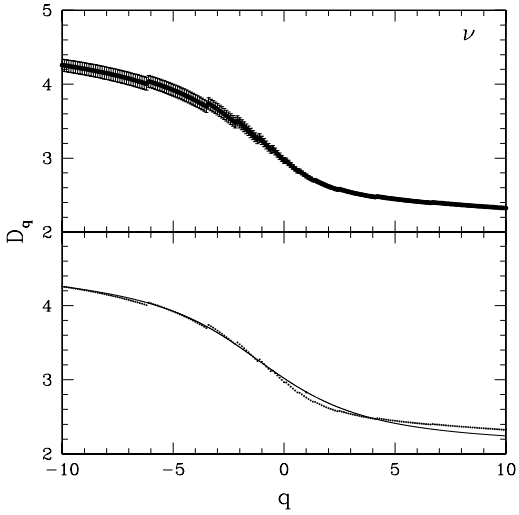

Fig. 16 Spectrum of generalized dimensions with error bars (*upper panel*) for the ν state corresponding to embedded dimension $M = 3$. The lower panel shows the D_q values without error bars and the best fit curve.

the presence of colored noise. This is also true in the case of the other two identical states, λ and μ. Thus these three states could be a mixture of deterministic nonlinearity and colored noise. Thus, based on our results, the 12 states can be divided into three broader classes from the point of view of their temporal properties. It turns out that some of these states, which are spectroscopically different, behave identically in terms of their nonlinear dynamical characteristics. This may be an indication of some common features in the mechanism of production of light curves from these states. The temporal behavior of each state as obtained from our analysis is indicated in the last column in Table 1. Since the behavior is identical for two different observation IDs in all cases, it may be concluded that the results presented here are not dependent on sample selection and are applicable for all the light curves classified by Belloni et al. (2000).

Finally, we show the results of multifractal analysis of all the light curves except the four which show purely stochastic behavior and hence the $f(\alpha)$ spectrum is irrelevant. Our non subjective scheme for computing the D_q and $f(\alpha)$ spectrum, discussed in Section 2.4, provides us with a set of parameters that can be used to compare the fractal properties between different states as reflected in the light curves. To show the details of the computations, we first take a typical state. In Figure 16, we show the D_q spectrum for the ν state along with the best fit curve from which the $f(\alpha)$ is computed as given in Figure 17. This is repeated for the other states as well and the results for four other states are shown in Figure 18. The multifractal nature of the attractors is evident from the figures. Since the computation is done under fixed conditions prescribed by the algorithmic scheme, the associated parameters characterizing the spectra can give a better representation for comparison between various states. Our results indicate that the spectra and the associated parameters are typically different for each state and do not show any clear trend among members that display strong deterministic nonlinear behavior. This can be inferred from Figure 18 for the case of different ranges of scales. Thus, it turns out that there are subtle differences between the states belonging to the same dynamic class with respect to multifractal scaling as well, apart from linear spectral characteristics, based on which the 12 states are divided.

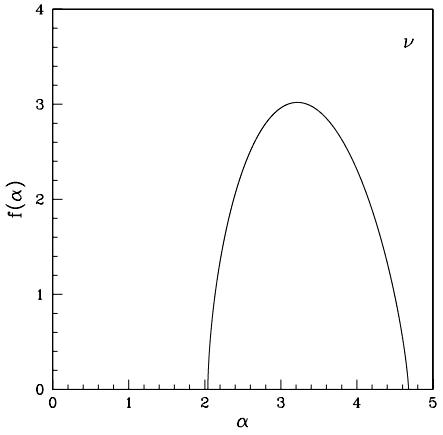

Fig. 17 Multifractal spectrum for the ν state computed from the best fit curve for D_q shown in the previous figure.

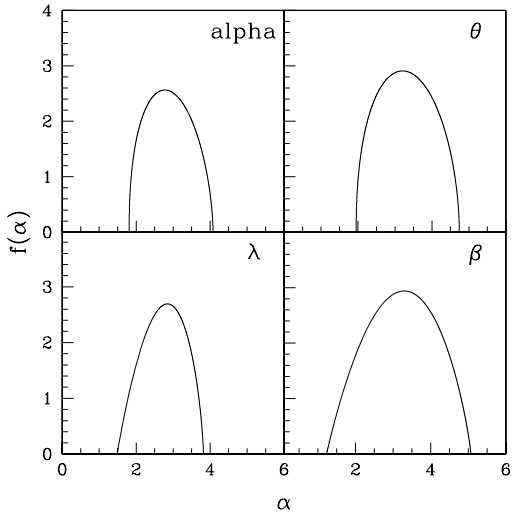

Fig. 18 $f(\alpha)$ spectrum for the light curves corresponding to four states of the black hole system computed using our scheme with $M = 3$. Note that the GRS state has been labeled *alpha* in order to avoid confusion with the scaling index α.

4 DISCUSSION AND CONCLUSIONS

Identifying nontrivial structures in real world systems is considered to be a challenging task as it requires a succession of tests using various quantitative measures. Even though a large number of potential systems from various fields have been analyzed so far, the results remain inconclusive in many cases. Here we present an example of a very interesting astrophysical system, which we analyze using several important quantifiers of low dimensional chaos. By using the time series from

a standard chaotic system - the Rossler attractor - we first test the computational schemes used for the analysis. These schemes are then applied to the light curves from the black hole system. We find that out of the 12 spectroscopic states, only four are purely stochastic. The remaining show signatures of deterministic nonlinearity, with three of them contaminated by colored noise. All these eight states are found to have $D_2 < 4$, so that their complex temporal behavior can be approximated by three or four coupled ordinary differential equations. Based on our results, the 12 states can be broadly classified into three from a dynamical perspective: purely stochastic with $D_2 \rightarrow \infty$, affected by colored noise and those which are potential candidates for low dimensional $(D_2 < 4)$ chaotic behavior.

It should be noted that Belloni et al. (2000) classified the light curves into 12 states based on their count rate, variability and spectral characteristics. In other words, this is a classification based on linear characteristics of the light curves. Ours is not a classification as in the strict sense of Belloni et al. (2000). We only show that some of the light curves which appear different based on their variability and spectral properties can be grouped together when viewed from a dynamical perspective.

Our results could be significant in many ways. First of all, this is the first real evidence of a possible multifractal attractor in the time series of a black hole system. The fact that the light curves from many of the temporal states have underlying strange-attractor-like behavior increases the possibility that the temporal variability in the time scales within these states are governed by some inherently nonlinear processes with a few degrees of freedom. In other words, the complex nonlinear partial differential equations that are known to govern the hydrodynamic flow can be approximated by a set of ordinary differential equations and hence can be more easily studied and understood. Moreover, the result that some of the states which are spectroscopically different, but have approximately the same nonlinear characteristics, is interesting from certain dynamical aspects, such as the mechanism of production of light curves. It is well known that GRS1915+105 is a unique black hole system with many temporal states which vary over a wide range of time scales. Many of the questions regarding this variability and the exact mechanism of production of light curves still remain unanswered.

Another question is regarding the structure of variability between the 12 spectroscopic states. It has been suggested that all the observed light curves could be interpreted in terms of three basic states (a hard state and two softer states) and a sequence of transitions between them (Belloni et al. 2000). This could, in principle, give rise to a much larger variety of light curves. However, the system chooses only a handful of these sequences. This possibly suggests that the structure of time variability is not random, but controlled by some physical parameter which must be connected to the basic properties of the accretion disk. The presence of deterministic nonlinear behavior in the system further substantiates this idea.

Interestingly, the system appears to be in the χ state for most of the time which is identified as purely stochastic in our analysis. We have also analyzed many samples of the long time average of the light curves from the system and found that they show purely random behavior. Thus, one possibility is that the states other than the χ state may well be short-time *flips* due to some changes taking place within the system. However, many of these short-time states acquire much less noise, which reveals, for example, the underlying nonlinear character. Thus, an interesting question is whether the states such as β and θ have a different underlying mechanism of production of light curves compared to the χ state; or, is it the case that the excessive amount of white noise in that state is what suppresses the nonlinear properties? The question whether the different states are temporal manifestations of a single underlying mechanism or are they dynamically different, will be vital for a proper modeling of this fascinating astrophysical object.

Acknowledgements KPH and RM acknowledge the financial support from the Dept. of Sci. and Tech., Govt. of India, through a Research Grant No. SR/S2/HEP - 11/2008. KPH acknowledges the hospitality and computing facilities in IUCAA, Pune.

References

Aberbanel, H. D. L. 1996, Analysis of Observed Chaotic Data (New York: Springer)
Athanasiu, M. A., & Pavlos, G. P. 2001, Nonlinear Processes in Geophys., 8, 95
Atmanspacher, H., Demmel, V., Morfill, G., Scheingraber, H., Voges W., & Wiedenmann, G. 1989a, in Measures of Complexity and Chaos, eds. Abraham, N. B., Albano, A. M., Passamante, A., & Rapp, R. E. (New York: Plenum Press)
Atmanspacher, H., Scheingraber, H., & Wiedenmann, G. 1989b, Phys. Rev. A, 40, 3954
Belloni, T., Klein-Wolt, M., Mendez, M., van der Klis, M., & van Paradjis, J. 2000, A&A, 355, 271
Broomhead, D. S., & King, G. P. 1986, Physica D, 20, 217
Gliozzi, M., Papadakis, I. E., & Rath, C. 2006, A&A, 449, 969
Gliozzi, M., Rath, C., Papadakis, I. E., & Reig, P. 2010, A&A, 512, 21
Grassberger, P., & Procaccia, I. 1983, Phys. Rev. Lett., 50, 346
Halsey, T. C., Jensen, M. H., Kadanoff, L. P., Procaccia, I., & Shraimann, B. I. 1986, Phys. Rev. A, 33, 1141
Harikrishnan, K. P., Misra, R., & Ambika, G. 2009a, Comm. Nonlinear Sci. Num. Simulations, 14, 3608
Harikrishnan, K. P., Misra, R., Ambika, G., & Amritkar, R. E. 2009b, Chaos, 19, 043129
Harikrishnan, K. P., Misra, R., Ambika, G., & Amritkar, R. E. 2010, Physica D, 239, 420
Harikrishnan, K. P., Misra, R., Ambika, G., & Kembhavi, A. K. 2006, Physica D, 215, 137
Hegger, R., Kantz, H., & Schreiber, T. 1999, Chaos, 9, 413
Hentschel, H. G. E., & Procaccia, I. 1983, Physica D, 8, 435
Hilborn, R. C. 1994, Chaos and Nonlinear Dynamics (New York: Oxford University Press)
Hongre, L., Sailhac, P., Alexandrescu, M., & Dubois, J. 1999, Physics of Earth and Planet. Int., 110, 157
Jevtic, N., Zelechoski, S., Feldman, H., Peterson, C., & Schweitzer, J. S. 2005, ApJ, 635, 527
Kantz, H., & Schreiber, T. 1997, Nonlinear Time Series Analysis (Cambridge: Cambridge University Press)
Karak, B. B., Dutta, J., & Mukhopadhyay, B. 2010, ApJ, 708, 862
Kennel, M. B., & Isabelle, R. 1992, Phys. Rev. A, 46, 3111
Kugiumtzis, D. 1999, Phys. Rev. E, 60, 2808
Lakshmanan, M., & Rajasekar, S. 2003, Nonlinear Dynamics (New York: Springer)
Misra, R., Harikrishnan, K. P., Ambika, G., & Kembhavi, A. K. 2006, ApJ, 643, 1114
Misra, R., Harikrishnan, K. P., Mukhopadhyay, B., Ambika, G., & Kembhavi, A. K. 2004, ApJ, 609, 313
Norris, J. P., & Matilsky, T. A. 1989, ApJ, 346, 912
Ott, E. 1993, Chaos in Dynamical Systems (Cambridge: Cambridge Univ. Press)
Redaelli, S., Plewczynki, D., & Macek, W. M. 2002, Phys. Rev. E, 66, 035202(R)
Sauer, T., Yorke, J., & Casdagli, M. 1991, J. Stat. Phys., 65, 579
Schreiber, T. 1999, Phys. Reports, 308, 1
Schreiber, T., & Schmitz, A. 1996, Phys. Rev. Lett., 77, 635
Schreiber, T., & Schmitz, A. 2000, Physica D, 142, 346
Sprott, J. C. 2003, Chaos and Time Series Analysis (New York: Oxford University Press)
Takens, F. 1981, Lecture Notes in Mathematics, Vol. 898 (New York: Springer)
Theiler, J., Eubank, S., Longtin, A., Galdrikian, B., & Farmer, J. D. 1992, Physica D, 58, 77
Timmer, J., Schwarz, U., Voss, H. U., Wardinski, I., Belloni, T., Hasinger, G., van der Klis, M., & Kurths, J. 2000, Phys. Rev. E, 61, 1342
Uttley, P., McHardy, I. M., & Vaughan, S. 2005, MNRAS, 359, 345
Voges,W., Atmanspacher, H., & Scheingraber, H. 1987, ApJ, 320, 794